
MoE-SPAC: EFFICIENT MoE INFERENCE BASED ON SPECULATIVE ACTIVATION UTILITY IN HETEROGENEOUS EDGE SCENARIOS

Shuhuai Li
 Shanghai University
 Shanghai, China
 lishuhuai_brian@shu.edu.cn

Jianghao Lin*
 Shanghai Jiao Tong University
 Shanghai, China
 linjianghao@sjtu.edu.cn

Dongdong Ge
 Shanghai Jiao Tong University
 Shanghai, China
 dge@sjtu.edu.cn

Yinyu Ye
 Stanford University
 California, United States
 yyeye@stanford.edu

ABSTRACT

Mixture-of-Experts (MoE) models enable scalable performance but face severe memory constraints on edge devices. Existing offloading strategies struggle with I/O bottlenecks due to the dynamic, low-information nature of autoregressive expert activation. In this paper, we propose to repurpose Speculative Decoding (SD) not merely as a compute accelerator, but as an informative *lookahead sensor* for memory management, supported by our theoretical and empirical analyses. Hence, we introduce **MoE-SpAc**, an MoE inference framework that integrates a *Speculative Utility Estimator* to track expert demand, a *Heterogeneous Workload Balancer* to dynamically partition computation via online integer optimization, and an *Asynchronous Execution Engine* to unify the prefetching and eviction in the same utility space. Extensive experiments on seven benchmarks demonstrate that MoE-SpAc achieves a **42%** improvement in TPS over the SOTA SD-based baseline, and an average **4.04×** speedup over all standard baselines. Code is available at <https://github.com/lshAlgorithm/MoE-SpAc>.

1 Introduction

Large Language Models (LLMs) have achieved remarkable capabilities by scaling to hundreds of billions or even trillions of parameters [1, 2, 3]. The Mixture-of-Experts (MoE) architecture has been instrumental in this growth, offering a path to vastly larger models while keeping the computational cost manageable [4, 5, 6]. By routing each input token through only a small subset of expert networks, MoE dramatically reduces the required floating-point operations (FLOPs), compared to dense models of similar size.

However, this parameter efficiency imposes a severe memory penalty. The immense parameter footprint creates a critical barrier to deployment in resource-constrained environments, such as personal devices and edge hardware. To

this end, *heterogeneous offloading* has become the standard solution. Typically, the full set of expert weights resides in high-capacity CPU memory, while activated experts are transferred on-demand to the high-throughput GPU device.

Existing offloading strategies generally fall into two categories. *The first* strategy involves **GPU intensive** expert calculation. It offloads activated expert weights from CPU to GPU on demand, which significantly exacerbates the I/O bottleneck between heterogeneous devices [7]. While predictive *prefetching* attempts to hide this latency using auxiliary networks [8, 9] or historical activation¹ patterns [10, 11], these methods suffer from unavoidable prediction errors due to the binary, low-information signals during the autoregressive (AR) generation. *The second* strategy is **CPU-GPU hybrid** expert calculation, which

*Corresponding author.

¹In this paper, unless otherwise specified, “activation” refers to the MoE gating decision (i.e., which experts are selected).

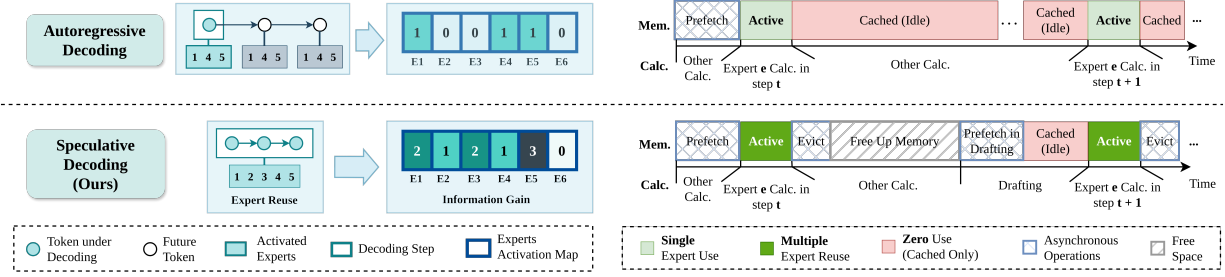


Figure 1: The advantages of speculative decoding (SD, Bottom) compared with traditional autoregressive decoding (AR, Top) from both theoretical (Left) and practical (Right) perspectives. Theoretically, SD enables expert reuse and transforms binary, low-information AR signals into informative frequency-valued ones. Practically, MoE-SpAc masks I/O latency by asynchronously prefetching experts during the drafting phase, unlike AR which suffers from blocking loads.

allows CPU execution of experts that are missed in GPU VRAM to reduce expert loading overhead. Fiddler [12] and kTransformers [13] adopt this method but rely on static expert allocation or profiling, failing to capture the dynamic nature of expert activation [14]. Although HybriMoE [15] introduces a dynamic strategy, its prefetching and caching algorithms remain decoupled, preventing a unified scheduling objective and resulting in suboptimal load balancing [16].

In this paper, we identify a novel synergy between speculative decoding (SD) [17, 18] and heterogeneous MoE inference. We propose to repurpose SD not merely as an accelerator, but as an informative lookahead sensor for memory management. Typically, SD accelerates inference by using a smaller draft model to generate candidate tokens, which the larger target model verifies in a parallel forward pass. As shown in Figure 1, we observe that the SD paradigm offers decisive advantages for MoE inference from both theoretical and practical aspects.

Theoretically, SD *reuses* the expert weights and *enriches* the transmission of expert activation signals. As shown in Figure 1(Left), while autoregressive decoding yields a binary indicator (activated or not) for a single step, the verification of multiple draft tokens generates a richer expert *activation frequency map* that reflects the expert utility trend over the immediate future context. Hence, SD transforms the low-information binary signals of autoregressive decoding into non-binary, informative signals for expert scheduling. Furthermore, SD introduces inherent *fault tolerance*: exact frequency prediction is unnecessary; coarse-grained utility scores are sufficient to guide effective scheduling policies.

Practically, as shown in Figure 1(Right), SD enables *parallel scheduling*, where experts can be prefetched to GPU without interference while the system processes the draft phase. Additionally, it presents an opportunity to optimize *heterogeneous compute utilization*: by offloading low-frequency experts to the CPU (sequential processing), we reserve the high-throughput GPU for high-frequency experts like E5 on left of Figure 1 (parallel processing),

thereby balancing the load effectively across heterogeneous devices.

Leveraging these insights, we propose **MoE-SpAc**, an efficient **MoE** inference framework based on **speculative activation utility** in heterogeneous edge scenarios. Rather than treating SD merely as a computation accelerator, MoE-SpAc introduces a *Speculative Utility Estimator*. This estimator evaluates expert demand in a stable, discrete utility space via an inertial transition mechanism. Guided by these utilities, a *Heterogeneous Workload Balancer* solves an online integer optimization problem at each layer, dynamically determining a global threshold to partition experts between GPU and CPU based on real-time I/O and memory constraints. These decisions are executed by an *Asynchronous Execution Engine*, which unifies prefetching and eviction under the same utility metric to minimize synchronization overhead. In this way, MoE-SpAc not only masks I/O latency but also harmonizes the computational load across heterogeneous hardware, transforming the memory wall into a manageable expert scheduling problem.

In summary, our contributions are as follows:

- **Paradigm Shift:** We redefine the role of speculative decoding in MoE inference, shifting its paradigm from a mere computation accelerator to an informative *lookahead sensor* for memory management, which is supported by both theoretical and empirical analysis.
- **Unified Scheduling Framework.** We propose *MoE-SpAc*, which integrates speculative decoding for online heterogeneous expert scheduling based on unified expert utilities. MoE-SpAc dynamically harmonizes CPU-GPU workloads, ensuring optimal throughput by adapting to strict I/O and memory constraints in real-time.
- **SOTA Performance:** Extensive experiments on seven benchmarks demonstrate that MoE-SpAc achieves a **42%** speedup in TPS over the best SD-based baseline, effectively breaking the memory wall for efficient MoE inference in edge scenarios.

2 Preliminary and Problem Formulation

2.1 Speculative Decoding

Speculative Decoding (SD) accelerates inference by leveraging a lightweight *draft model* to generate a sequence of γ candidate tokens, which are verified in parallel by the larger *target model*. This parallelism maximizes GPU compute utilization compared to the serial nature of autoregressive decoding, generating $[1, \gamma + 1]$ tokens at once. Let α denote the acceptance probability of a draft token. The expected number of tokens generated per decoding step, $\Omega(\gamma, \alpha)$, is given by Leviathan et al. [17]:

$$\Omega(\gamma, \alpha) := \mathbb{E}[\# \text{ Generated Tokens}] = \frac{1 - \alpha^{\gamma+1}}{1 - \alpha}. \quad (1)$$

The latency of generating $\Omega(\gamma, \alpha)$ tokens using speculative decoding (T_{SD}) or autoregressive decoding (T_{AR}) is:

$$\begin{aligned} T_{SD} &= \gamma \cdot T_D + T_V, \\ T_{AR} &= \Omega(\gamma, \alpha) \cdot T_V, \end{aligned} \quad (2)$$

where T_D is the time for the draft model to generate a single token, and T_V is the latency of a single parallel verification pass by the target model. Hence, the wall-clock speedup factor is $T_{AR}/T_{SD} = \frac{1 - \alpha^{\gamma+1}}{(1 - \alpha)(\gamma c + 1)}$, where $c = T_D/T_V$ represents the cost coefficient.

2.2 Mixture-of-Experts Architecture

Unlike dense models that utilize all parameters for every forward pass, MoE models conditionally activate only a subset of parameters per token. Formally, let $\mathbf{h} \in \mathbb{R}^d$ denote the input hidden state for a token at a specific MoE layer. This layer contains a set of N experts, $\mathcal{E} = \{E_1, E_2, \dots, E_N\}$, where each expert $E_i(\cdot)$ is typically a feed-forward network (FFN). The output \mathbf{y} is the weighted aggregation of activated experts under a Top- k ($k \ll N$) routing strategy:

$$\begin{aligned} \mathbf{s} &= \mathbf{W}_g \mathbf{h} \in \mathbb{R}^N \\ \mathcal{T}(\mathbf{h}) &= \text{Top-}k(\mathbf{s}) \subset \{1, \dots, N\}, \\ g_i(\mathbf{h}) &= \frac{\exp(\mathbf{s}_i)}{\sum_{j \in \mathcal{T}(\mathbf{h})} \exp(\mathbf{s}_j)}, \quad i \in \mathcal{T}(\mathbf{h}), \\ \mathbf{y} &= \sum_{i \in \mathcal{T}(\mathbf{h})} g_i(\mathbf{h}) \cdot E_i(\mathbf{h}), \end{aligned} \quad (3)$$

where $\mathbf{W}_g \in \mathbb{R}^{N \times d}$ is the learnable routing matrix, $\mathcal{T}(\mathbf{h})$ is the indices of k activated experts. and $g_i(\mathbf{h})$ is the normalized weight for expert E_i . Thus, the majority ($N - k$) of experts remain inactive, creating significant sparsity.

2.3 Online Heterogeneous Expert Scheduling

We formalize the efficient inference of MoE models on memory-constrained edge devices as an online decision-making problem, termed *Heterogeneous Expert Scheduling*. The objective is to dynamically prioritize high-

frequency experts (hot) to GPU while offloading the computation of low-frequency experts (cold) to CPU at each inference step to minimize the I/O-induced latency.

Inference Step. Let t denote a discrete inference step to generate a sequence of tokens \mathbf{X}_t . In autoregressive (AR) decoding, a step t corresponds to the generation of a single token, i.e., $|\mathbf{X}_t| = 1$. In speculative decoding (SD), a step t corresponds to a verification cycle that potentially generates multiple tokens, i.e., $\mathbb{E}|\mathbf{X}_t| = \Omega(\gamma, \alpha) \geq 1$.

Activation Frequency. For a given step t and input tokens \mathbf{X}_t , we define the *observed* activation frequency $f_{i,t}$ for expert E_i as the cumulative number of times that E_i is activated in Eq. 3 over tokens \mathbf{X}_t . For AR, $f_{i,t} \in \{0, 1\}$, providing a low-information, binary signal. For SD, $f_{i,t} \in [0, \gamma + 1]$, providing a more informative, non-binary signal that reflects the *intensity* of expert demand.

Expert Utility Estimation. To guide the expert scheduling, it requires a metric of expert priority for the *upcoming* step $t + 1$. Let $s_{i,t+1}$ denote the *ground-truth utility score*, which is determined by a monotonically non-decreasing mapping function $G(\cdot)$ applied to the future (unknown) frequency:

$$s_{i,t+1} = G(f_{i,t+1}), \quad (4)$$

where $G(\cdot)$ maps frequencies to a discrete utility space (e.g., priority levels). Since $f_{i,t+1}$ is unobservable at step t , we must estimate the future utility $\hat{s}_{i,t+1}$ using a scoring function F based on the current utility and historical frequencies:

$$\hat{s}_{i,t+1} = F(\hat{s}_{i,t}, \{f_{i,j}\}_{j=1}^t). \quad (5)$$

Heterogeneous Resource Allocation. The final scheduling decision is a thresholding operation on estimated utilities. Let τ_t be a dynamic threshold determined by the system's resource constraints at step t . We partition the experts as:

- **Hot Experts** ($\hat{s}_{i,t+1} \geq \tau_t$): Experts with high activation frequency across the speculative window should be prioritized (prefetched) for high-throughput GPU.
- **Cold Experts** ($\hat{s}_{i,t+1} < \tau_t$): Experts with negligible or zero activation should be evicted from GPU to CPU-side execution for load balancing.

Compared with existing works, we provide a new perspective on scheduling, including prefetching and eviction based on a unified standard, i.e. utility score based on speculative decoding. By introducing the score at step level rather than request level during SD, we can implement online load balancing considering heterogeneous computation and memory capacity for MoE inference.

Moreover, we theoretically demonstrate that beyond simple speedup, SD fundamentally alters the nature of the online heterogeneous expert scheduling by providing *Expert Reuse*, *Information Gain*, and *Fault Tolerance* in Appendix A.

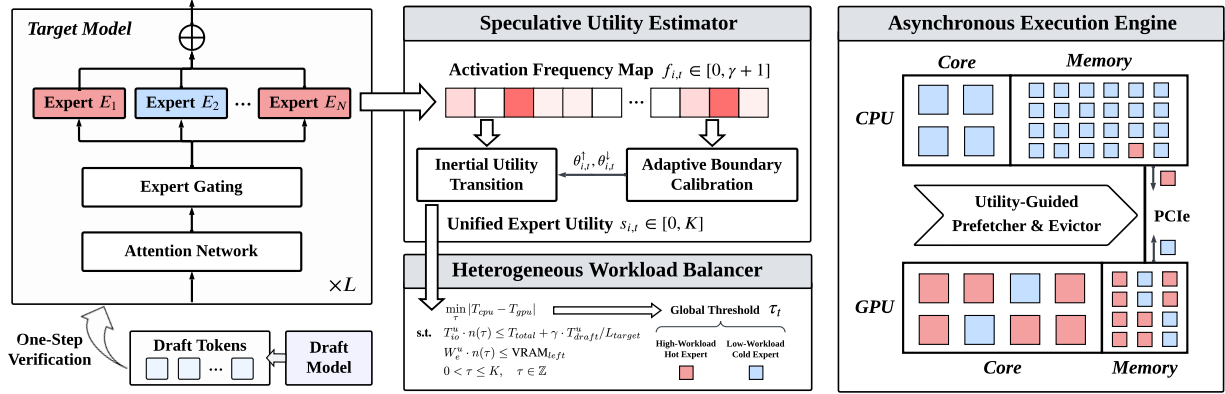


Figure 2: Overall framework of MoE-SpAc.

3 MoE-SpAc

3.1 Overview

To resolve the online heterogeneous expert scheduling problem, we present **MoE-SpAc**, an efficient **MoE** inference framework based on **Speculative Activation** utility for edge scenarios.

As shown in Figure 2, MoE-SpAc consists of three key components: (1) *Speculative Utility Estimator* predicts future expert demand for each verification step based on inertial utility transition and adaptive boundary calibration; (2) *Heterogeneous Workload Balancer* harmonizes computation loads between devices by solving layer-wise online integer optimization to determine the optimal global threshold for GPU-CPU expert partitioning; and (3) *Asynchronous Execution Engine* actualizes prefetching and eviction decisions based on a *unified* utility metric, managing I/O operations asynchronously without stalling the critical computation. In this way, we adapt speculative decoding to MoE inference in edge scenarios, not merely as a compute accelerator, but also as a core lookahead sensor for critical memory management between heterogeneous devices.

3.2 Speculative Utility Estimator

To effectively guide the heterogeneous scheduling, we have to derive an expert utility score that is both reflective of *next-step demand* and robust against *frequency fluctuations*. Due to the temporal locality and smooth evolving of the accumulated activation frequencies across speculative windows, we estimate the expert utility in a compressed discrete space, i.e., $s_{i,t} \in \{0, \dots, K\}$, where $K \leq \gamma$ is the utility upper bound. Here, $s_{i,t} = 0$ indicates a dormant (extremely cold) expert, while $s_{i,t} = K$ represents a fully saturated (extremely hot) expert. As illustrated in Algorithm 1, we conduct *speculative utility estimation* based on the historical activation frequencies at each verification step t , which consists of two key components: *inertial utility transition* and *adaptive boundary calibration*.

Algorithm 1 Speculative Utility Estimation

- 1: **Hyperparameters:** Utility Upper Bound K , Number of Experts N , Forgetting Factor λ .
 - 2: **Initialize:** Utility $s_{i,1} = 0$ for all $i \in \{1, \dots, N\}$.
 - 3: **Initialize:** Boundaries $\theta_{i,1}^\uparrow = \theta_{i,1}^\downarrow = \lfloor \gamma/2 \rfloor$.
 - 4: **for** inference step $t = 1, 2, \dots$ **do**
 - 5: Observe activation frequencies $\mathbf{f}_t = \{f_{1,t}, \dots, f_{N,t}\}$
 - 6: **for** each expert $i \in \{1, \dots, N\}$ **do**
 - 7: $\Delta_{i,t} \leftarrow f_{i,t} - f_{i,t-1}$ ▷ Calculate Fluctuation
 - 8: // **Inertial Utility Transition**
 - 9: **if** $\Delta_{i,t} \geq \theta_{i,t}^\uparrow$ **then**
 - 10: $s_{i,t+1} \leftarrow \min(K, s_{i,t} + 1)$
 - 11: **else if** $-\Delta_{i,t} \geq \theta_{i,t}^\downarrow$ **then**
 - 12: $s_{i,t+1} \leftarrow \max(0, s_{i,t} - 1)$
 - 13: **else**
 - 14: $s_{i,t+1} \leftarrow s_{i,t}$
 - 15: **end if**
 - 16: // **Adaptive Boundary Calibration**
 - 17: **if** $\Delta_{i,t} > 0$ **then**
 - 18: $\theta_{i,t+1}^\uparrow \leftarrow [(1 - \lambda)\theta_{i,t}^\uparrow + \lambda \cdot \Delta_{i,t}]$
 - 19: $\theta_{i,t+1}^\downarrow \leftarrow \theta_{i,t}^\downarrow$
 - 20: **else if** $\Delta_{i,t} < 0$ **then**
 - 21: $\theta_{i,t+1}^\uparrow \leftarrow \theta_{i,t}^\uparrow$
 - 22: $\theta_{i,t+1}^\downarrow \leftarrow [(1 - \lambda)\theta_{i,t}^\downarrow + \lambda \cdot |\Delta_{i,t}|]$
 - 23: **else**
 - 24: $\theta_{i,t+1}^\uparrow \leftarrow \theta_{i,t}^\uparrow$; $\theta_{i,t+1}^\downarrow \leftarrow \theta_{i,t}^\downarrow$
 - 25: **end if**
 - 26: **end for**
 - 27: **end for**
-

Inertial Utility Transition. To better estimate the utility score dynamically, we introduce an inertial update mechanism. At each step t , the utility score $s_{i,t}$ of expert E_i remains unchanged unless the frequency fluctuation, de-

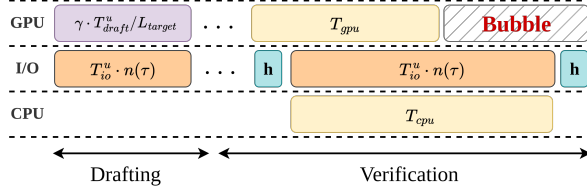


Figure 3: Pipeline of single layer forward in SD scenario. GPU and CPU stands for calculation on each device. h in I/O stands for the transmission of hidden states of tokens. Note that the T_{io}^* stands for the prefetching time for **another** layer, and here is simplified for clarity.

defined as $\Delta_{i,t} = f_{i,t} - f_{i,t-1}$, exceeds a significant margin². Formally, the transition is governed by:

$$s_{i,t+1} \leftarrow \begin{cases} \min(K, s_{i,t} + 1) & \text{if } \Delta_{i,t} \geq \theta_{i,t}^\uparrow \\ \max(0, s_{i,t} - 1) & \text{if } -\Delta_{i,t} \geq \theta_{i,t}^\downarrow \\ s_{i,t} & \text{otherwise} \end{cases} \quad (6)$$

where $\theta_{i,t}^\uparrow$ and $\theta_{i,t}^\downarrow$ are expert-specific fluctuation boundaries at step t to trigger the utility transition upward (+1) or downward (-1). This inertia ensures that the system only incurs the high I/O cost of prefetching or eviction when there is a sustained shift in expert demand, effectively filtering out high-frequency noise.

Adaptive Boundary Calibration. The boundaries are initialized as $\lfloor \gamma/2 \rfloor$, but should be adaptively calibrated at each step to reflect the evolving trend of expert demand inertia. As shown in Algorithm 1, according to the positivity of frequency fluctuation, we update the boundaries via a moving average with a forgetting factor λ . In this way, the system adapts to the current workload characteristics, maintaining high responsiveness during distribution shifts while preserving stability during steady processes.

We provide more empirical and theoretical analysis to support the design rationale of speculative utility estimation in Appendix B.

3.3 Heterogeneous Workload Balancer

With the expert utilities estimated above, now we have to determine the optimal global threshold τ_t that separates hot experts (prioritized on GPU) from cold experts (processed on CPU). Inspired by Chen et al. [16], we model this as an online integer optimization problem, solved for *each Transformer layer* of the target model at *each verification step*. For brevity, we omit the subscripts for step t and layer l in the following formulation. Table 1 summarizes the key notations used in our formulation.

Objective. As shown in Figure 3, our goal is to balance the computation load between heterogeneous devices to

²Since the inertial utility transition does not require fitting to a ground-truth utility score, we denote the estimated utility as $s_{i,t}$, instead of $\hat{s}_{i,t}$ for simplicity.

Table 1: Notations for heterogeneous workload balancing. The subscripts for step t and layer l are omitted for brevity.

Symbol	Description
τ	The decision variable of the dynamic threshold to partition the hot and cold experts.
γ	The number of speculative tokens, i.e., draft length.
k	The number of experts to be activated for the MoE layer, i.e., the top- k routing strategy.
b	The number of de-duplicated activated experts for the γ draft tokens. Note that $b \leq \gamma \cdot k$ due to expert reuse.
$n(\tau)$	The number of experts to be prefetched, i.e., hot experts ($s \geq \tau$) that are not on GPU.
$r_c(\tau)$	The ratio of γk activated experts to be <i>sequentially</i> processed on CPU. This ratio has to be <i>estimated</i> based on historical signals.
$r_g(\tau)$	The ratio of b de-duplicated activated experts to be processed on GPU <i>in parallel</i> . This ratio has to be <i>estimated</i> based on historical signals.
T_{cpu}^u, T_{gpu}^u	The unit inference time for an activated expert on CPU / GPU.
T_{io}^u	The unit I/O transmission time for loading a single expert.
T_{draft}^u	The unit inference time for the draft model to generate one token.
L_{target}	The number of Transformer layers for the target model.
W_e^u	The unit memory space required to store a single expert.
VRAM_{left}	The real-time available VRAM capacity for caching experts.

minimize synchronization overhead (bubbles). With notations from Table 1, we can derive the total expert execution times for CPU (T_{cpu}) and GPU (T_{gpu}), respectively:

$$T_{cpu} = r_c(\tau) \cdot \gamma \cdot k \cdot T_{cpu}^u, \quad (7)$$

$$T_{gpu} = r_g(\tau) \cdot b \cdot T_{gpu}^u. \quad (8)$$

The system latency is dominated by the bottleneck device: $T_{total} = \max(T_{cpu}, T_{gpu})$. Hence, the objective is to minimize the difference between execution times of heterogeneous devices, i.e., $|T_{cpu} - T_{gpu}|$.

Constraints. The solution must satisfy the following constraints. (1) *I/O Constraint*: the time used to prefetch $n(\tau)$ new experts to GPU must not exceed the available computation window. As a bonus brought by SD, we can prefetch during the drafting phase. (2) *Memory Constraint*: the total size of newly prefetched experts must fit within the remaining VRAM. (3) *Decision Variable Constraint*: the decision variable τ should fall in the discrete utility space.

Formulation. Combining the objective and constraints, the complete optimization problem is formulated as:

$$\min_{\tau} |T_{cpu} - T_{gpu}| \quad (9)$$

$$\text{s.t. } T_{io}^u \cdot n(\tau) \leq T_{total} + \gamma \cdot T_{draft}^u / L_{target} \quad (10)$$

$$W_e^u \cdot n(\tau) \leq \text{VRAM}_{left} \quad (11)$$

$$0 < \tau \leq K, \quad \tau \in \mathbb{Z} \quad (12)$$

Since the objective function is convex with respect to τ and the feasible set is a contiguous integer range $[1, K]$, the optimal threshold τ^* can be determined in $O(1)$ time

complexity by evaluating the function at the analytical root and the feasibility boundaries. The detailed formulation and solution derivation is provided in Appendix C due to the page limitation.

3.4 Unified Asynchronous Execution Engine

To actualize the optimal threshold τ derived by the heterogeneous workload balancer, it requires an efficient mechanism to physically migrate expert weights without stalling the computation pipeline. Hence, we design an *asynchronous execution engine* that orchestrates prefetching and eviction based on the *unified* utility score $s_{i,t}$.

Utility-Guided Prefetching. To manage the prefetching requests, we implement a *multi-level priority queue*, where each level contains pending requests for experts with the same utility $s_{i,t}$. Within each level, requests follow a First-In-First-Out (FIFO) order to respect the temporal sequence of layer execution for target model. The prefetcher continuously scans the queues at different levels in descending order of utility (from K down to τ). The execution logic is filtered by the dynamic threshold τ_t : the prefetcher only processes queues with levels $s_{i,t} \geq \tau_t$, transferring weights in descending order of priority (from level K down to τ).

Utility-Guided Eviction. Complementarily, we manage the resident GPU cache using a *state-ordered pool*, implemented via a Red-Black tree. This structure indexes all GPU-resident experts by their current utility score $s_{i,t}$. When the load balancer updates the threshold to τ_t , the evictor can efficiently identify and remove resident experts with decreased scores $s_{i,t} < \tau_t$ in $O(\log N)$ time.

Crucially, unlike traditional policies such as Adaptive Replacement Cache [19] or Least Recently Used (LRU) [20] which rely on historical access timestamps, our approach employs a **unified metric** (expert utility) for both prefetching and eviction. This unification ensures scheduling consistency, effectively preventing the cache thrashing of marginally hot experts.

Implementation details regarding the CUDA streams and thread management are provided in Appendix D.

4 Experiments

4.1 Experiment Setups

Hardware. We evaluate MoE-SpAc under constrained resources with a single NVIDIA GeForce RTX 4090 GPU, connected to CPU memory via a PCIe 4.0 interface (32GB/s).

Benchmarks. We adopt diverse benchmarks to cover different capabilities of LLMs, including MMLU-Pro [21], MT-bench [22], HumanEval [23], GSM8K [24], Alpaca [25], CNN/DailyMail [26], and QA [27].

Baselines. The baselines fall into two categories. (1) General inference engines, including Accelerate [28], vLLM [29], and llama.cpp [30]. (2) Inference sys-

tems tailored for MoE models, including Mixtral Offloading [31], MoE-Infinity [11], SP-MoE [32], Fate [33], and HybriMoE [15]. Detailed descriptions of each baseline are given in Appendix E.

Implementation Details. We employ the MoE model Qwen3-30B-A3B as the target verifier and a quantized dense model Qwen3-4B-FP8 as the draft model [34]. The thinking mode is enabled for deep reasoning on MMLU-Pro benchmark only. We set the hyperparameters as follows: draft length $\gamma = 8$, forgetting factor $\lambda = 0.1$, and utility upper bound $K = 4$. The expert cache ratio on GPU VRAM is set to 17%. The maximum number of generated tokens per step is set to 512. Following previous works [11, 32, 35], we use a batch size of 1 to simulate edge deployment, where inference is typically single-request and memory-constrained. The hyperparameters of other baselines are carefully tuned for fair comparison.

Metric. We adopt tokens per second (TPS) and latency (Lat.) as evaluation metrics, which capture the end-to-end efficiency of the inference system.

4.2 Overall Performance

Table 2 reports the tokens per second (TPS) and latency performance of different inference methods. We can observe that MoE-SpAc consistently outperforms all baselines with an average **4.04 \times** speedup in TPS, establishing a new SOTA of MoE inference engines in memory-constrained edge scenarios. Moreover, even compared against the best baseline llama.cpp-w/SD, which is also optimized with speculative decoding, MoE-SpAc still achieves a **41.9%** relative improvement in TPS metric on average. This validates the gains derived specifically from our online heterogeneous expert scheduling policy to mitigate the memory bottleneck, rather than the computational speedup from SD alone.

To further analyze the model compatibility and generalization of our proposed MoE-SpAc, we compare it against the best baselines from both categories (llama.cpp-w/SD and HybriMoE) based on DeepSeek-V2-Lite [36] with int4 quantized one as draft model. The results are reported in Table 3. MoE-SpAc consistently outperforms baselines by a large margin, achieving averaged 52.9% improvement in TPS, and 45.6% on latency. This demonstrates that our proposed MoE-SpAc is highly generalized and compatible with different MoE models.

4.3 Information Gain from Speculative Decoding

To illustrate the information gain brought by SD for expert utility estimation, we report the hot-or-cold online prediction accuracy of MoE-SpAc (SD) and HybriMoE (AR) on MMLU-Pro in Figure 4. The experiments are conducted on the 47th layer of the MoE model. Since the decoding length per step is different between SD and AR, we report the averaged accuracy of HybriMoE as the dashed line. The threshold τ is set to 1 to facilitate AR. We observe that

Table 2: The tokens per second (TPS) and latency (Lat.) performance of different inference methods. The best results are given in **bold** while the second-best values are underlined. *Rel.Imprv.* indicates the relative improvement of MoE-SpAc against the best baseline.

Method	MMLU-Pro		MT-bench		GSM8K		HumanEval		Alpaca		CNN/DM		QA		Average	
	TPS↑	Lat.↓														
Accelerate	1.13	495.37	1.15	435.55	1.21	237.45	1.15	393.60	1.09	350.83	1.27	222.47	1.16	138.42	1.17	324.81
vLLM	2.65	203.74	2.67	187.88	2.67	94.63	2.63	158.46	2.67	137.72	2.57	104.28	2.68	57.43	2.65	134.88
llama.cpp	15.17	37.92	14.34	36.08	15.01	19.21	14.74	30.57	16.86	22.40	15.42	19.46	15.09	11.07	15.23	25.24
llama.cpp-w/ SD	<u>17.29</u>	<u>32.88</u>	<u>17.58</u>	<u>29.03</u>	<u>19.03</u>	<u>15.09</u>	<u>18.78</u>	<u>24.01</u>	<u>18.02</u>	<u>21.51</u>	<u>16.46</u>	<u>18.36</u>	<u>16.49</u>	<u>10.43</u>	<u>17.66</u>	<u>21.62</u>
Mixtral Offload	2.43	230.87	2.36	212.70	2.35	120.25	2.48	177.87	2.33	162.32	2.23	131.72	2.33	70.86	2.36	158.08
MoE-Infinity	3.64	151.43	3.64	136.84	3.63	75.42	3.63	119.53	3.48	107.82	3.56	80.56	3.44	46.13	3.57	102.53
SP-MoE	4.75	116.73	4.46	111.34	4.87	55.78	4.98	86.93	4.83	76.16	4.38	65.24	4.55	34.62	4.69	78.11
Fate	7.93	73.65	7.89	66.89	7.82	39.42	7.82	60.24	7.42	54.83	7.83	40.78	7.83	24.23	7.79	51.43
HybriMoE	12.22	47.62	12.03	43.47	12.38	24.83	11.96	38.18	12.29	32.46	12.37	25.11	11.83	15.45	12.15	32.45
MoE-SpAc (Ours)	25.80	23.11	24.10	22.26	27.82	11.34	28.24	16.93	23.15	17.88	22.78	14.31	23.56	8.36	25.06	16.31
<i>Rel.Imprv.</i>	49.2%	29.7%	37.1%	23.3%	46.2%	24.8%	50.4%	29.5%	28.5%	16.9%	38.4%	22.1%	42.9%	19.8%	41.9%	24.6%

Table 3: The model compatibility analysis of our proposed MoE-SpAc based on DeepSeek-V2-Lite model.

Method	MT-bench		HumanEval		CNN/DM	
	TPS↑	Lat.↓	TPS↑	Lat.↓	TPS↑	Lat.↓
HybriMoE	18.43	33.32	17.95	24.16	18.43	21.78
llama.cpp-w/ SD	30.78	21.83	30.49	17.85	33.23	15.94
MoE-SpAc (Ours)	47.10	12.66	47.26	9.46	50.17	8.13
<i>Rel.Imprv.</i>	53.0%	42.0%	55.0%	47.0%	51.0%	49.0%

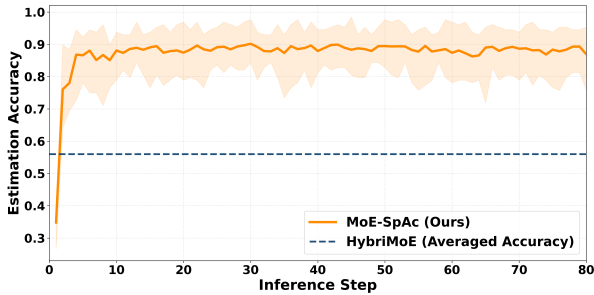


Figure 4: The hot-or-cold online prediction accuracy of MoE-SpAc (SD) and HybriMoE (AR) on MMLU-Pro. Since the decoding length per step is different between SD and AR, we report the averaged accuracy of HybriMoE as the dashed line.

MoE-SpAc can quickly learn the activation patterns and steadily achieve prediction accuracy around 0.85, which is superior to traditional AR-based utility modeling like HybriMoE.

4.4 Ablation Study

To impact of each component in MoE-SpAc, we conduct the ablation study on MMLU-Pro, HumanEval, and CNN/DM benchmarks. We define the variants as follows: (1) w/o SpecUE removes speculative utility estimator, falling back to binary utility modeling with $K = 1$; (2) w/o AdaBC removes adaptive boundary calibration and uses fixed boundaries ($\theta_{i,t}^\uparrow = 3, \theta_{i,t}^\downarrow = 1$); (3) w/o HetWB removes heterogeneous workload balancer and employs a

Table 4: Ablation study of MoE-SpAc.

Model Variants	MMLU-Pro		HumanEval		CNN/DM	
	TPS↑	Lat.↓	TPS↑	Lat.↓	TPS↑	Lat.↓
MoE-SpAc (Full)	25.80	23.11	28.24	16.93	22.78	14.31
w/o SpecUE	19.53	29.48	20.56	25.27	18.43	19.53
w/o AdaBC	25.33	23.48	28.03	19.03	22.31	15.98
w/o HetWB	24.32	24.32	26.95	19.97	20.16	17.69
w/o SG-Prefetcher	17.27	32.91	18.79	27.44	16.46	21.23
w/o SG-Evictor	18.31	31.23	20.03	25.72	17.16	21.01
w/o SD (AR Mode)	17.25	32.95	16.43	30.13	15.97	22.44

static threshold ($\tau = 2$) instead of solving the online optimization; (4) w/o SG-Prefetcher removes score-guided prefetcher, falling back to static expert allocation; (5) w/o SG-Evictor removes score-guided evictor by retaining experts until VRAM is full; (6) w/o SD removes speculative decoding, reverting to standard autoregressive inference. The results are summarized in Table 4, from which we obtain the following observations:

- The speculative utility estimator is the cornerstone of our framework. Removing it (i.e., w/o SpecUE) results in a significant drop in both throughput and latency, confirming that the informative frequency-valued signals brought by SD are crucial for expert demand estimation and memory management.
- Within the estimator, the adaptive boundary calibration contributes to robustness. However, its removal (w/o AdaBC) yields only a marginal degradation. This suggests that our default parameters ($\theta^\uparrow = 3, \theta^\downarrow = 1$) are sufficiently general for most expert activation patterns, though adaptation refines performance for corner cases.
- The heterogeneous workload balancer proves critical for I/O management. By fixing the threshold τ , the system fails to adapt to real-time I/O bandwidth constraints, leading to either I/O congestion or under-utilization of the GPU, causing a performance drop.
- The score-guided prefetcher and evictor are tightly coupled. Removing one of them degrades the performance to the level of the baseline, since I/O is no longer masked. This confirms that the synergy between predictive scor-

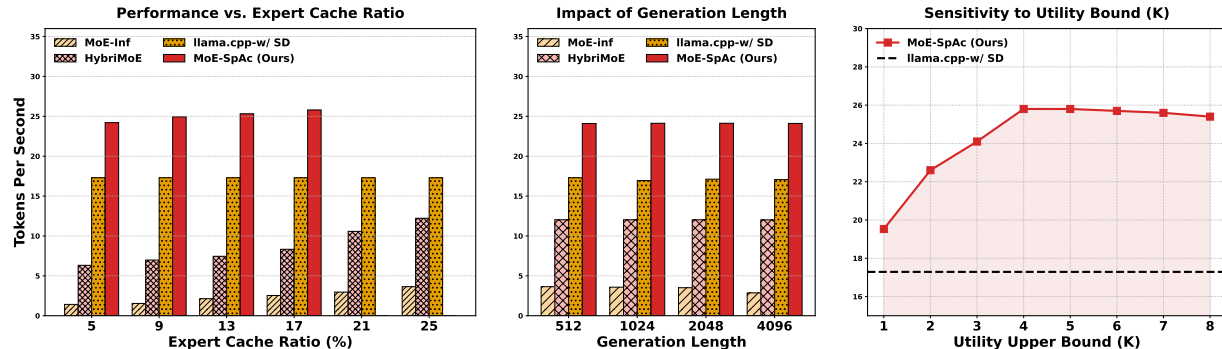


Figure 5: Stability and sensitivity analysis. Left: Impact of expert cache ratios; despite an OOM boundary at 21% due to draft model allocation, MoE-SpAc yields superior throughput compared to existing works. Middle: Scalability across generation lengths, showing consistent gains over baselines in long-context tasks. Right: Effect of the threshold cap K , where small values reduce performance by limiting the precision of the utility score.

ing, dynamic balancing, and asynchronous execution is essential for realizing the full potential of MoE-SpAc.

4.5 In-Depth Analysis

As shown in Figure 5, we analyze the sensitivity and stability of MoE-SpAc to variations in critical system resources and configurations, including expert cache ratio (Left), generation length (Mid), and utility upper bound (Right).

Expert Cache Ratio. We illustrate the performance impact of varying the GPU VRAM allocated for expert weights in the left of Figure 5. We have the following observations:

- As the expert cache ratio decreases, the AdaBC in MoE-SpAc responds to the tightening VRAM constraint in Eq. 11 by increasing the threshold τ . This forces the system to offload a larger proportion of marginal experts to the CPU, yielding stable and significantly better throughput performance compared to baselines.
- The draft model itself imposes a static memory overhead (around 8%), preventing MoE-SpAc from allocating as much VRAM to the expert cache as the baselines (triggering OOM at a 21% cache ratio in our setup). However, this memory “investment” for draft model in SD yields a high return: MoE-SpAc with a restricted expert cache (e.g., 17%) still outperforms baselines operating with significantly larger cache allocations (e.g., 25%).

Generation Length. In Figure 5 (Mid), we expand the maximum generation length from 512 to 4096. MoE-SpAc consistently outperforms baselines by a large margin across different generation lengths. This stability indicates that the overheads of our speculative utility estimator and AdaBC are constant rather than cumulative, allowing the latency benefits of heterogeneous scheduling to be amortized effectively over long-horizon generation tasks.

Utility Upper Bound K . On the right of Figure 5, we vary the utility upper bound K from 1 to 8 and report the TPS performance. Small values ($K < 4$) lead to performance

degeneration due to the imprecise scoring and shrunken solution space for τ . Larger K do not show much loss in performance, and our choice of $K = 4$ is the most efficient for online computing.

5 Related Work

Efficient MoE on the Edge. While Mixture-of-Experts (MoE) architectures are essential for scaling LLMs, their size often exceeds edge GPU memory. Compression techniques like pruning [37, 38] and quantization [39, 40] trade generation quality for speed. Consequently, system-level offloading has become a preferred alternative. To mitigate the high I/O overhead of on-demand loading, recent systems employ *Expert Prefetching* [11, 41] to look ahead at activation patterns, or *Expert Caching* [42, 43] to retain frequently accessed experts in high-bandwidth memory.

Speculative Decoding (SD) and Heterogeneous Computing. SD [17] reduces latency by verifying drafted tokens in parallel. While SD is computationally expensive in large-batch regimes, it is ideal for memory-bound edge scenarios (small batches), where verification arithmetic is masked by memory retrieval time [44]. To further address resource constraints, heterogeneous computing allows CPU offloading. Systems like Fiddler [12] and kTransformers [13] execute expert layers on the CPU only during cache misses, while HybriMoE [15] reorders experts to dispatch “cold” computations to the CPU. However, these approaches often rely on greedy algorithms or lack theoretical foundations for optimal resource distribution.

Concurrent Developments. Recent studies exploring SD for MoE [45, 46] often rely on simplified assumptions, such as uniformly activated experts, or focus on throughput rather than latency. Furthermore, existing work [32, 47] often overlooks continuous activation trends and remains constrained to GPU-centric execution.

More detailed related works are provided in Appendix G.

6 Conclusion

We introduce *MoE-SpAc*, an MoE inference framework that extends the role of speculative decoding from a compute accelerator into an informative lookahead sensor for heterogeneous memory management in edge scenarios. We design an online heterogeneous expert scheduling policy based on unified expert utility. Empirical results on seven benchmarks demonstrate that MoE-SpAc effectively mitigates the memory bottleneck, achieving a 42% improvement over the SOTA SD-based baseline and an average $4.04\times$ speedup over all standard baselines. Future work involves extending the principle of speculative utility estimation to emerging sparse architectures like Mixture-of-Lookup-Experts to further advance efficient edge memory management.

Impact Statement

This paper presents work whose goal is to advance the field of machine learning. There are many potential societal consequences of our work, none of which we feel must be specifically highlighted here.

References

- [1] T. Brown, B. Mann, N. Ryder, M. Subbiah, J. D. Kaplan, P. Dhariwal, A. Neelakantan, P. Shyam, G. Sastry, A. Askell *et al.*, “Language models are few-shot learners,” *Advances in neural information processing systems*, vol. 33, pp. 1877–1901, 2020.
- [2] L. Ouyang, J. Wu, X. Jiang, D. Almeida, C. Wainwright, P. Mishkin, C. Zhang, S. Agarwal, K. Slama, A. Ray *et al.*, “Training language models to follow instructions with human feedback,” *Advances in neural information processing systems*, vol. 35, pp. 27 730–27 744, 2022.
- [3] J. Achiam, S. Adler, S. Agarwal, L. Ahmad, I. Akkaya, F. L. Aleman, D. Almeida, J. Altschmidt, S. Altman, S. Anadkat *et al.*, “Gpt-4 technical report,” *arXiv preprint arXiv:2303.08774*, 2023.
- [4] R. A. Jacobs, M. I. Jordan, S. J. Nowlan, and G. E. Hinton, “Adaptive mixtures of local experts,” *Neural computation*, vol. 3, no. 1, pp. 79–87, 1991.
- [5] Y. Zhou, T. Lei, H. Liu, N. Du, Y. Huang, V. Zhao, A. M. Dai, Q. V. Le, J. Laudon *et al.*, “Mixture-of-experts with expert choice routing,” *Advances in Neural Information Processing Systems*, vol. 35, pp. 7103–7114, 2022.
- [6] S. Roller, S. Sukhbaatar, J. Weston *et al.*, “Hash layers for large sparse models,” *advances in neural information processing systems*, vol. 34, pp. 17 555–17 566, 2021.
- [7] Z. Fang, Z. Hong, Y. Huang, Y. Lyu, W. Chen, Y. Yu, F. Yu, and Z. Zheng, “Accurate expert predictions in moe inference via cross-layer gate,” *arXiv e-prints*, pp. arXiv–2502, 2025.
- [8] Z. Du, S. Li, Y. Wu, X. Jiang, J. Sun, Q. Zheng, Y. Wu, A. Li, H. Li, and Y. Chen, “Sida: Sparsity-inspired data-aware serving for efficient and scalable large mixture-of-experts models,” *Proceedings of Machine Learning and Systems*, vol. 6, pp. 224–238, 2024.
- [9] R. Hwang, J. Wei, S. Cao, C. Hwang, X. Tang, T. Cao, and M. Yang, “Pre-gated moe: An algorithm-system co-design for fast and scalable mixture-of-expert inference,” in *2024 ACM/IEEE 51st Annual International Symposium on Computer Architecture (ISCA)*. IEEE, 2024, pp. 1018–1031.
- [10] J. Li, Y. Jiang, Y. Zhu, C. Wang, and H. Xu, “Accelerating distributed {MoE} training and inference with lina,” in *2023 USENIX Annual Technical Conference (USENIX ATC 23)*, 2023, pp. 945–959.
- [11] L. Xue, Y. Fu, Z. Lu, L. Mai, and M. Marina, “Moe-infinity: Activation-aware expert offloading for efficient moe serving,” *arXiv preprint arXiv:2401.14361*, vol. 3, 2024.
- [12] K. Kamahori, Y. Gu, K. Zhu, and B. Kasikci, “Fiddler: Cpu-gpu orchestration for fast inference of mixture-of-experts models,” 2024.
- [13] H. Chen, W. Xie, B. Zhang, J. Tang, J. Wang, J. Dong, S. Chen, Z. Yuan, C. Lin, C. Qiu, Y. Zhu, Q. Ou, J. Liao, X. Chen, Z. Ai, Y. Wu, and M. Zhang, “Ktransformers: Unleashing the full potential of cpu/gpu hybrid inference for moe models,” in *Proceedings of the ACM SIGOPS 31st Symposium on Operating Systems Principles*, 2025.
- [14] E. Yu, Z. Zhang, D. Dong, Y. Wu, and X. Liao, “Prescope: Unleashing the power of prefetching for resource-constrained moe inference,” *arXiv preprint arXiv:2509.23638*, 2025.
- [15] S. Zhong, Y. Sun, L. Liang, R. Wang, R. Huang, and M. Li, “Hybrimoe: Hybrid cpu-gpu scheduling and cache management for efficient moe inference,” *arXiv preprint arXiv:2504.05897*, 2025.
- [16] Z. Chen, T. Bu, C. Song, X. Lu, Y. Ye, and Z. Zhou, “A universal load balancing principle and its application to large language model serving,” *arXiv preprint arXiv:2601.17855*, 2026.
- [17] Y. Leviathan, M. Kalman, and Y. Matias, “Fast inference from transformers via speculative decoding,” in *International Conference on Machine Learning*. PMLR, 2023, pp. 19 274–19 286.
- [18] H. Xia, T. Ge, P. Wang, S.-Q. Chen, F. Wei, and Z. Sui, “Speculative decoding: Exploiting speculative execution for accelerating seq2seq generation,” *arXiv preprint arXiv:2203.16487*, 2022.
- [19] N. Megiddo and D. S. Modha, “Outperforming lru with an adaptive replacement cache algorithm,” *Computer*, vol. 37, no. 4, pp. 58–65, 2004.

- [20] M. Chrobak and J. Noga, “Lru is better than fifo,” *Algorithmica*, vol. 23, no. 2, pp. 180–185, 1999.
- [21] Y. Wang, X. Ma, G. Zhang, Y. Ni, A. Chandra, S. Guo, W. Ren, A. Arulraj, X. He, Z. Jiang *et al.*, “Mmlu-pro: A more robust and challenging multi-task language understanding benchmark,” *Advances in Neural Information Processing Systems*, vol. 37, pp. 95 266–95 290, 2024.
- [22] L. Zheng, W.-L. Chiang, Y. Sheng, S. Zhuang, Z. Wu, Y. Zhuang, Z. Lin, Z. Li, D. Li, E. Xing *et al.*, “Judging llm-as-a-judge with mt-bench and chatbot arena,” *Advances in neural information processing systems*, vol. 36, pp. 46 595–46 623, 2023.
- [23] M. Chen, J. Tworek, H. Jun, Q. Yuan, H. P. D. O. Pinto, J. Kaplan, H. Edwards, Y. Burda, N. Joseph, G. Brockman *et al.*, “Evaluating large language models trained on code,” *arXiv preprint arXiv:2107.03374*, 2021.
- [24] K. Cobbe, V. Kosaraju, M. Bavarian, M. Chen, H. Jun, L. Kaiser, M. Plappert, J. Tworek, J. Hilton, R. Nakano *et al.*, “Training verifiers to solve math word problems,” *arXiv preprint arXiv:2110.14168*, 2021.
- [25] R. Taori, I. Gulrajani, T. Zhang, Y. Dubois, X. Li, C. Guestrin, P. Liang, and T. B. Hashimoto, “Stanford alpaca: An instruction-following llama model,” https://github.com/tatsu-lab/stanford_alpaca, 2023.
- [26] R. Nallapati, B. Zhou, C. Gulcehre, B. Xiang *et al.*, “Abstractive text summarization using sequence-to-sequence rnns and beyond,” *arXiv preprint arXiv:1602.06023*, 2016.
- [27] T. Kwiatkowski, J. Palomaki, O. Redfield, M. Collins, A. Parikh, C. Alberti, D. Epstein, I. Polosukhin, J. Devlin, K. Lee *et al.*, “Natural questions: a benchmark for question answering research,” *Transactions of the Association for Computational Linguistics*, vol. 7, pp. 453–466, 2019.
- [28] T. Wolf, L. Debut, V. Sanh, J. Chaumond, C. Delangue, A. Moi, P. Cistac, T. Rault, R. Louf, M. Funtowicz *et al.*, “Huggingface’s transformers: State-of-the-art natural language processing,” *arXiv preprint arXiv:1910.03771*, 2019.
- [29] W. Kwon, Z. Li, S. Zhuang, Y. Sheng, L. Zheng, C. H. Yu, J. Gonzalez, H. Zhang, and I. Stoica, “Efficient memory management for large language model serving with pagedattention,” in *Proceedings of the 29th symposium on operating systems principles*, 2023, pp. 611–626.
- [30] Ollama, “Ollama,” <https://github.com/ollama/ollama>, 2025, accessed: 2025-09-14.
- [31] A. Eliseev and D. Mazur, “Fast inference of mixture-of-experts language models with offloading,” *arXiv preprint arXiv:2312.17238*, 2023.
- [32] L. Chen, Z. Wen, T. Wu, X. Zhang, and C. Wu, “Sp-moe: Speculative decoding and prefetching for accelerating moe-based model inference,” *arXiv preprint arXiv:2510.10302*, 2025.
- [33] Z. Fang, Z. Hong, Y. Huang, Y. Lyu, W. Chen, Y. Yu, F. Yu, and Z. Zheng, “Fate: Fast edge inference of mixture-of-experts models via cross-layer gate,” *arXiv preprint arXiv:2502.12224*, 2025.
- [34] A. Yang, A. Li, B. Yang, B. Zhang, B. Hui, B. Zheng, B. Yu, C. Gao, C. Huang, C. Lv *et al.*, “Qwen3 technical report,” *arXiv preprint arXiv:2505.09388*, 2025.
- [35] R. Svirshchevski, A. May, Z. Chen, B. Chen, Z. Jia, and M. Ryabinin, “Specexec: Massively parallel speculative decoding for interactive llm inference on consumer devices,” *Advances in Neural Information Processing Systems*, vol. 37, pp. 16 342–16 368, 2024.
- [36] DeepSeek-AI, “Deepseek-v2: A strong, economical, and efficient mixture-of-experts language model,” 2024.
- [37] Y. Xie, Z. Zhang, D. Zhou, C. Xie, Z. Song, X. Liu, Y. Wang, X. Lin, and A. Xu, “Moe-pruner: Pruning mixture-of-experts large language model using the hints from its router,” *arXiv preprint arXiv:2410.12013*, 2024.
- [38] J. Lee, A. Qiao, D. F. Campos, Z. Yao, Y. He *et al.*, “Stun: Structured-then-unstructured pruning for scalable moe pruning,” *arXiv preprint arXiv:2409.06211*, 2024.
- [39] E. Frantar and D. Alistarh, “Qmoe: Practical sub-1-bit compression of trillion-parameter models,” *arXiv preprint arXiv:2310.16795*, 2023.
- [40] H. Imani, A. Amirany, and T. El-Ghazawi, “Mixture of experts with mixture of precisions for tuning quality of service,” in *2024 IEEE International Conference on Rebooting Computing (ICRC)*. IEEE, 2024, pp. 1–6.
- [41] S. Zhong, L. Liang, Y. Wang, R. Wang, R. Huang, and M. Li, “Adapmoe: Adaptive sensitivity-based expert gating and management for efficient moe inference,” in *Proceedings of the 43rd IEEE/ACM International Conference on Computer-Aided Design*, 2024, pp. 1–9.
- [42] X. He, S. Zhang, Y. Wang, H. Yin, Z. Zeng, S. Shi, Z. Tang, X. Chu, I. Tsang, and O. Y. Soon, “Expertflow: Optimized expert activation and token allocation for efficient mixture-of-experts inference,” *arXiv preprint arXiv:2410.17954*, 2024.
- [43] P. Tang, J. Liu, X. Hou, Y. Pu, J. Wang, P.-A. Heng, C. Li, and M. Guo, “Hobbit: A mixed precision expert offloading system for fast moe inference,” *arXiv preprint arXiv:2411.01433*, 2024.
- [44] T. Cai, Y. Li, Z. Geng, H. Peng, J. D. Lee, D. Chen, and T. Dao, “Medusa: Simple llm inference acceleration framework with multiple decoding heads,” *arXiv preprint arXiv:2401.10774*, 2024.

- [45] Z. Huang, L. Zhu, Z. Zhan, T. Hu, W. Mao, X. Yu, Y. Liu, and T. Zhang, “Moesd: Unveil speculative decoding’s potential for accelerating sparse moe,” *arXiv preprint arXiv:2505.19645*, 2025.
- [46] Z. Wang, Z. Zhang, Y. Zhou, Z. Wang, M. Zhou, P. Jiang, W. Cai, C. Huan, R. Gu, S. Zhong *et al.*, “Accelerating mixture-of-experts inference by hiding offloading latency with speculative decoding,” *arXiv preprint arXiv:2508.21706*, 2025.
- [47] W. Wang, J. Liu, X. Hou, X. Xia, P. Tang, M. Zhang, C. Li, and M. Guo, “Moe-speq: Speculative quantized decoding with proactive expert prefetching and offloading for mixture-of-experts,” *arXiv preprint arXiv:2511.14102*, 2025.
- [48] Y. Li, F. Wei, C. Zhang, and H. Zhang, “Eagle: Speculative sampling requires rethinking feature uncertainty,” *arXiv preprint arXiv:2401.15077*, 2024.
- [49] O. Dietrich, J. G. Raya, S. B. Reeder, M. F. Reiser, and S. O. Schoenberg, “Measurement of signal-to-noise ratios in mr images: influence of multichannel coils, parallel imaging, and reconstruction filters,” *Journal of Magnetic Resonance Imaging: An Official Journal of the International Society for Magnetic Resonance in Medicine*, vol. 26, no. 2, pp. 375–385, 2007.
- [50] H. Kim, G. Papamakarios, and A. Mnih, “The lipschitz constant of self-attention,” in *International Conference on Machine Learning*. PMLR, 2021, pp. 5562–5571.
- [51] S. Agrawal, Z. Wang, and Y. Ye, “A dynamic near-optimal algorithm for online linear programming,” *Operations Research*, vol. 62, no. 4, pp. 876–890, 2014.
- [52] X. Li, C. Sun, and Y. Ye, “Simple and fast algorithm for binary integer and online linear programming,” *Advances in Neural Information Processing Systems*, vol. 33, pp. 9412–9421, 2020.
- [53] S. Markidis, S. W. Der Chien, E. Laure, I. B. Peng, and J. S. Vetter, “Nvidia tensor core programmability, performance & precision,” in *2018 IEEE international parallel and distributed processing symposium workshops (IPDPSW)*. IEEE, 2018, pp. 522–531.
- [54] F. C. Salinas, K. Kumatani, R. Gmyr, L. Liu, and Y. Shi, “Knowledge distillation for mixture of experts models in speech recognition,” Technical Report MSR-TR-2022-6, Microsoft Research, May 2022. <https://www...>, Tech. Rep., 2022.
- [55] F. Shu, Y. Liao, L. Zhuo, C. Xu, L. Zhang, G. Zhang, H. Shi, L. Chen, T. Zhong, W. He *et al.*, “Llava-mod: Making llava tiny via moe knowledge distillation,” *arXiv preprint arXiv:2408.15881*, 2024.
- [56] C. Yang, Y. Sui, J. Xiao, L. Huang, Y. Gong, Y. Duan, W. Jia, M. Yin, Y. Cheng, and B. Yuan, “Moe-i²: Compressing mixture of experts models through inter-expert pruning and intra-expert low-rank decomposition,” *arXiv preprint arXiv:2411.01016*, 2024.
- [57] P. Li, Z. Zhang, P. Yadav, Y.-L. Sung, Y. Cheng, M. Bansal, and T. Chen, “Merge, then compress: Demystify efficient smoe with hints from its routing policy,” *arXiv preprint arXiv:2310.01334*, 2023.
- [58] S. Cao, S. Liu, T. Griggs, P. Schafhalter, X. Liu, Y. Sheng, J. E. Gonzalez, M. Zaharia, and I. Stoica, “Moe-lightning: High-throughput moe inference on memory-constrained gpus,” in *Proceedings of the 30th ACM International Conference on Architectural Support for Programming Languages and Operating Systems, Volume 1*, 2025, pp. 715–730.
- [59] X. Zhuge, X. Shen, Z. Wang, F. Dang, X. Ding, D. Li, Y. Han, T. Hao, and Z. Yang, “Specoflood: Unlocking latent gpu capacity for llm inference on resource-constrained devices,” *arXiv preprint arXiv:2505.10259*, 2025.
- [60] Z. Fang, Y. Huang, Z. Hong, Y. Lyu, W. Chen, Y. Yu, F. Yu, and Z. Zheng, “Klowski: Efficient mixture-of-expert inference via expert-aware multi-batch pipeline,” in *Proceedings of the 30th ACM International Conference on Architectural Support for Programming Languages and Operating Systems, Volume 2*, 2025, pp. 574–588.
- [61] T. Xu, L. Xue, Z. Lu, A. Jackson, and L. Mai, “Moe-gen: High-throughput moe inference on a single gpu with module-based batching,” *arXiv preprint arXiv:2503.09716*, 2025.
- [62] Y. Xi, H. Wang, B. Chen, J. Lin, M. Zhu, W. Liu, R. Tang, Z. Wei, W. Zhang, and Y. Yu, “Efficiency unleashed: Inference acceleration for llm-based recommender systems with speculative decoding,” in *Proceedings of the 48th International ACM SIGIR Conference on Research and Development in Information Retrieval*, 2025, pp. 1891–1901.
- [63] Y. Zhang, “A markov categorical framework for language modeling,” *arXiv preprint arXiv:2507.19247*, 2025.
- [64] X. Liu, C. Daniel, L. Hu, W. Kwon, Z. Li, X. Mo, A. Cheung, Z. Deng, I. Stoica, and H. Zhang, “Optimizing speculative decoding for serving large language models using goodput,” *arXiv preprint arXiv:2406.14066*, 2024.
- [65] Y. Li, Y. Huang, B. Yang, B. Venkitesh, A. Locatelli, H. Ye, T. Cai, P. Lewis, and D. Chen, “Snapkv: Llm knows what you are looking for before generation,” *Advances in Neural Information Processing Systems*, vol. 37, pp. 22 947–22 970, 2024.
- [66] X. Miao, G. Oliaro, Z. Zhang, X. Cheng, Z. Wang, R. Y. Y. Wong, Z. Chen, D. Arfeen, R. Abhyankar, and Z. Jia, “Specinfer: Accelerating generative llm serving with speculative inference and token tree verification,” *arXiv preprint arXiv:2305.09781*, vol. 1, no. 2, p. 4, 2023.
- [67] H. Sun, Z. Chen, X. Yang, Y. Tian, and B. Chen, “Triforce: Lossless acceleration of long sequence gen-

- eration with hierarchical speculative decoding,” *arXiv preprint arXiv:2404.11912*, 2024.
- [68] D. Park and B. Egger, “Improving throughput-oriented llm inference with cpu computations,” in *Proceedings of the 2024 International Conference on Parallel Architectures and Compilation Techniques*, 2024, pp. 233–245.
- [69] Y. Song, Z. Mi, H. Xie, and H. Chen, “Powerinfer: Fast large language model serving with a consumer-grade gpu,” in *Proceedings of the ACM SIGOPS 30th Symposium on Operating Systems Principles*, 2024, pp. 590–606.
- [70] S. Li, H. Lu, T. Wu, M. Yu, Q. Weng, X. Chen, Y. Shan, B. Yuan, and W. Wang, “Caraserve: Cpu-assisted and rank-aware lora serving for generative llm inference,” *arXiv preprint arXiv:2401.11240*, 2024.
- [71] J. Zhang, J. Wang, H. Li, L. Shou, K. Chen, G. Chen, and S. Mehrotra, “Draft& verify: Lossless large language model acceleration via self-speculative decoding,” in *Proceedings of the 62nd Annual Meeting of the Association for Computational Linguistics (Volume 1: Long Papers)*, 2024, pp. 11 263–11 282.
- [72] R. Qin, Z. Li, W. He, J. Cui, H. Tang, F. Ren, T. Ma, S. Cai, Y. Zhang, M. Zhang *et al.*, “Mooncake: A kvcache-centric disaggregated architecture for llm serving,” *ACM Transactions on Storage*, 2024.
- [73] P. Jaillet, J. Jiang, K. Mellou, M. Molinaro, C. Podimata, and Z. Zhou, “Online scheduling for llm inference with kv cache constraints,” *arXiv preprint arXiv:2502.07115*, 2025.
- [74] S. Jie, Y. Tang, K. Han, Y. Li, D. Tang, Z.-H. Deng, and Y. Wang, “Mixture of lookup experts,” *arXiv preprint arXiv:2503.15798*, 2025.
- [75] X. Cheng, W. Zeng, D. Dai, Q. Chen, B. Wang, Z. Xie, K. Huang, X. Yu, Z. Hao, Y. Li, H. Zhang, H. Zhang, D. Zhao, and W. Liang, “Conditional memory via scalable lookup: A new axis of sparsity for large language models,” *arXiv preprint*, 2026. [Online]. Available: <https://arxiv.org/abs/2601.07372>

A Theoretical Analysis on Advantages of SD for MoE Inference

We analyze the theoretical advantages of speculative decoding (SD). We demonstrate that beyond simple speedup, SD fundamentally alters the nature of the online heterogeneous expert scheduling problem by providing *Expert Reuse*, *Information Gain*, and *Fault Tolerance*.

A.1 Expert Reuse

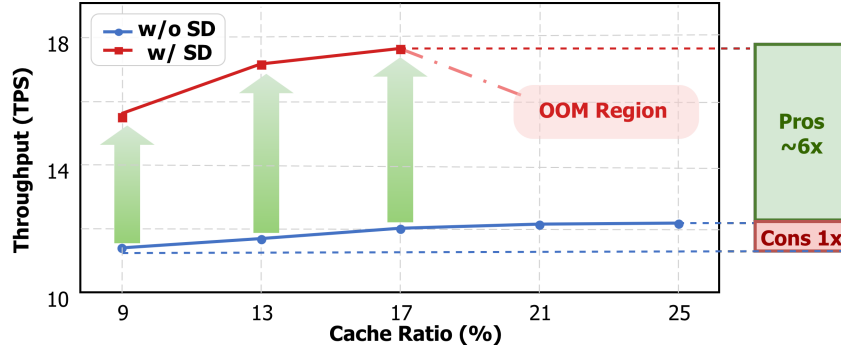


Figure 6: Illustration of TPS metric to the expert cache ratio(%) on NVIDIA GeForce RTX 4090 (24GB). Target model is Qwen3-30B-A3B, and draft one is Qwen3-4B-FP8. In edge scenario, less cache ratio precipitates only negligible decelerate, shown as red block with “Cons” label. Placing a small draft model can lead to huge speedup, shown as the green block with “Pros” label. Pros is about $6\times$ overweight Cons.

We first address the rationale for allocating scarce edge memory to a draft model rather than caching more experts. Figure 6 illustrates the Tokens Per Second (TPS) performance of Qwen3 models w.r.t. the percentage of total expert weights resident in GPU memory. The result reveals that marginally increasing the resident expert set yields diminishing returns in throughput for memory-bound regimes. Conversely, reserving a small partition of VRAM for a draft model (8% compared to all expert weights) enables SD, which unlocks substantial parallelism and expert reuse.

Although some works suggest SD is inefficient for MoE due to dynamic expert activation across different draft tokens [45, 48], we show that when γ (draft length) is tuned correctly, the *expert reuse* across the speculation window amortizes the loading cost. Aside from the original improvement in wall time, we now illustrate the scenario where the expert reuse in resource-constrained MoE architecture can achieve speedup.

Formally, following the notions in Section 2.1, T_V is dominated by FFN calculation, which is presented as

$$T = (k \cdot N) \cdot (T_{LOAD} + T_{FFN}) \cdot L, \quad (13)$$

where k is the coefficient of the proportion of the activated experts, N is the total number of experts needed for γ tokens, T_{LOAD} is the time for loading one expert, T_{FFN} is the time for calculating through one expert, and L is the number of layers.

Because of the *expert reuse*, ks for SD and AR are hard to describe with unified variable (not linear), thus denoting them as a and b , respectively. Therefore, we have

$$\begin{aligned} T_{SD} &= (a \cdot N) \cdot (T_{LOAD} + T_{FFN}) \cdot L + T_D \cdot \gamma \\ T_{AR} &= (b \cdot N) \cdot (T_{LOAD} + T_{FFN}) \cdot L \cdot \gamma \end{aligned} \quad (14)$$

For $N \cdot (T_{LOAD} + T_{FFN}) \cdot L$, which is constant, let us denote Z . Then the Time Per Output Token (TPOT) for both SD and AR is:

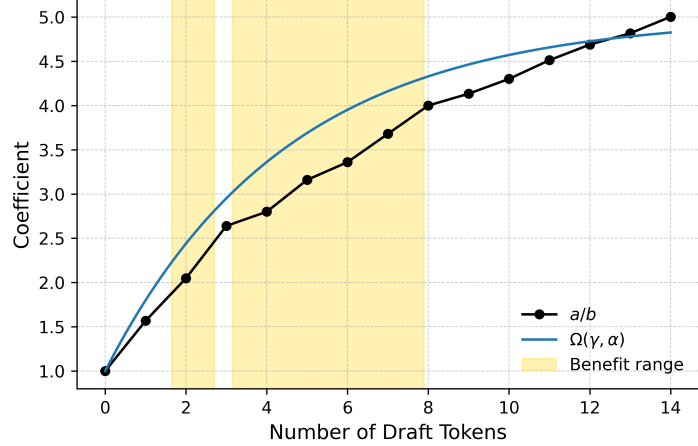
$$\begin{aligned} TPOT_{SD} &= \frac{Z \cdot a + \gamma \cdot T_D}{\Omega(\gamma, \alpha)} \\ TPOT_{AR} &= \frac{Z \cdot b \cdot \gamma}{\gamma} = Z \cdot b \end{aligned} \quad (15)$$

We next describe under which scenario, $TPOT_{SD} < TPOT_{AR}$ will be established, i.e.

$$a + \gamma \cdot \frac{T_D}{Z} < b \cdot \Omega(\gamma, \alpha) \quad (16)$$

γ	$\frac{a}{b}$
0	1
3	2.24
4	2.72
5	3.20
6	3.52
7	3.80
8	4.13
9	4.50
10	4.83
11	5.90
12	6.32

(a) Table on experimental data points.



(b) Experimental vs theoretical curve.

Figure 7: The curve comparison between $\Omega(\gamma, \alpha)$ and $\frac{a}{b}$, experimented on MT-bench with Qwen3-235B-A22B as verification model and Qwen3-4B-FP8, taking α as 0.8. (a) shows the numerical result, while (b) illustrates the benefit area.

Since $\gamma \cdot \frac{T_D}{Z}$ is relatively small, it suffices to guaranteed:

$$\frac{a}{b} < \Omega(\gamma, \alpha) \quad (17)$$

As Figure 7 illustrates for Qwen3 series, the advantage becomes more *pronounced* when $\gamma \in 2 \cup [3, 8]$. Thus, expert reuse benefits inference speed in theory and provide a guideline for setting the hyper-parameters.

Notice that $\Omega(\gamma, \alpha)$ has the limit:

$$\lim_{\gamma \rightarrow +\infty} \Omega(\gamma, \alpha) = \frac{1-0}{1-\alpha} = \frac{1}{1-\alpha} \quad (18)$$

which bounds the value of $\frac{a}{b}$ if an ideal speedup is desired.

Therefore, acceptance rate is closely related to the alignment between draft model and target model. A series of models which share the same pretraining data are ideal for off-shelf model speculation usage.

A.2 Information Gain

In Section 2.3, we illustrate how SD transforms the expert activation signals from binary indicators to frequency values. Here, we quantitatively demonstrate the information-theoretic advantage of this transformation.

Let $E_i(\cdot)$ be an expert with activation probability p_i . In standard AR inference, the expert activation for a single step is a random variable following a Bernoulli distribution: $X_i^{(1)} \sim \text{Bern}(p_i)$. In SD with a draft length γ , the activation generalizes to the aggregated count over the verification window, $X_i^{(\gamma+1)} = \sum_{t=1}^{\gamma+1} X_{i,t}^{(1)}$. By assuming weak inter-token correlation, this follows a Binomial distribution: $X_i^{(\gamma+1)} \sim \text{Bin}(\gamma+1, p_i)$.

Entropy Dominance. The Shannon entropy of the aggregated signal $X_i^{(\gamma+1)}$ strictly dominates that of $X_i^{(1)}$:

$$H(X_i^{(\gamma+1)}) = - \sum_{k=0}^{\gamma+1} p_k^{(\gamma+1)} \log p_k^{(\gamma+1)} \geq H(X_i^{(1)}) \quad (19)$$

where $p_k^{(\gamma+1)} = \Pr(X_i^{(\gamma+1)} = k)$. This implies that $X_i^{(\gamma+1)}$ carries strictly more bits of information regarding expert demand, reducing uncertainty for utility estimation.

Signal-to-Noise Ratio (SNR). The stability of the offloading signal is critical. Following Dietrich et al. [49], we define SNR as the ratio of the mean demand to its standard deviation (μ/σ). Then, we show that the SNR of expert activation

signals brought by SD is $\sqrt{\gamma+1}$ times more robust compared with that of standard AR decoding:

$$\begin{aligned} \text{SNR}_{AR} &= \frac{p_i}{\sqrt{p_i(1-p_i)}}, \\ \text{SNR}_{SD} &= \frac{(\gamma+1)p_i}{\sqrt{(\gamma+1)p_i(1-p_i)}} = \sqrt{\gamma+1} \cdot \text{SNR}_{AR} \end{aligned} \quad (20)$$

The relative noise in the SD signal decreases by a factor of $\sqrt{\gamma+1}$. This mathematical stabilization allows for reliable expert activation scoring, whereas AR is dominated by stochastic noise, especially when $p_i \ll 1$.

A.3 Fault Tolerance

Finally, we demonstrate that the transition from AR to SD relaxes the precision requirements of utility estimation with larger safety margins, granting the system fault tolerance.

Scheduling Fault. Recall from Section 2.3 that the scheduling decision depends on whether the estimated utility $\hat{s}_{i,t+1}$ exceeds the threshold τ_t . We define a *scheduling fault* \mathcal{E}_i as a discrepancy between the ground-truth optimal decision and the system’s derived decision:

$$\mathcal{E}_i = \mathbb{I}(\mathbb{I}(s_{i,t+1} \geq \tau_t) \neq \mathbb{I}(\hat{s}_{i,t+1} \geq \tau_t)), \quad (21)$$

Specifically, a fault corresponds to either a cache miss (False Negative) or memory waste (False Positive).

Safety Margin Analysis. We analyze the fault tolerance in frequency domain by defining τ_t^* as the frequency threshold, such that $G(f_{i,t+1}) \geq \tau_t \iff f_{i,t+1} \geq \tau_t^*$. Hence, a scheduling fault is avoided if the estimation error does not exceed the distance between the ground truth and the threshold, which is defined as the *safety margin* $\Delta_{i,t}$:

$$|\hat{f}_{i,t+1} - f_{i,t+1}| \leq \underbrace{|f_{i,t+1} - \tau_t^*|}_{\text{Safety Margin } \Delta_{i,t}} \Rightarrow \mathcal{E}_i = 0, \quad (22)$$

where $\hat{f}_{i,t+1}$ is the estimated frequency implied by the score.

AR Rigidity. In AR with $f_{i,t+1} \in \{0, 1\}$, the threshold typically lies in the interval $\tau_t^* \in (0, 1)$. Consequently, the safety margin is strictly bounded by $\Delta_{i,t} < 1$. Since frequency counts are integers, any prediction error implies $|\hat{f}_{i,t+1} - f_{i,t+1}| \geq 1 > \Delta_{i,t}$, inevitably causing a scheduling fault (e.g., predicting 0 when truth is 1).

SD Tolerance. In SD with $f_{i,t+1} \in [0, \gamma+1]$, the safety margin $\Delta_{i,t}$ can be larger than 1, especially for extremely hot or cold experts. For example, with $\gamma = 5$ and $\tau_t^* = 2$, an expert with demand $f_{i,t+1} = 5$ has a margin $\Delta_{i,t} = 3$. The system is tolerant to under-estimate the frequency by 1 or 2 units (noise) without crossing the boundary τ_t^* , still maintaining a correct scheduling decision ($\mathcal{E}_i = 0$).

B Design Rationale for Speculative Utility Estimation

In this section, we provide the analysis from the perspective of empirical observation and theoretical justification.

B.1 Empirical Observation

We construct a sequence of activation frequency of a same expert along the steps, e.g. $f_{1,0}, f_{1,2}, \dots, f_{1,t}$ for expert No.1. This sequences of different experts in speculative inference are depicted in Figure 8, with compared to those using AR. Empirically, these activation sequences in SD are more informative than AR and exhibit tighter correlation across steps. The frequency evolves gradually rather than fluctuate abruptly.

B.2 Theoretical Justification.

The validity of the Inertial Utility Transition relies on the premise that the underlying routing signal is smooth; otherwise, an inertial tracker would suffer from excessive lag. We formalize this smoothness via the bounded drift of expert gating scores.

Theorem 1. (*Bounded Drift of Expert Gating Scores*) Let $\mathbf{h}_t^{(0)}$ and $\mathbf{h}_{t+1}^{(0)}$ be the input embeddings for two consecutive inference steps with bounded initial divergence $\delta_{in} = \|\mathbf{h}_t^{(0)} - \mathbf{h}_{t+1}^{(0)}\|$. Assume the Attention and FFN modules in the

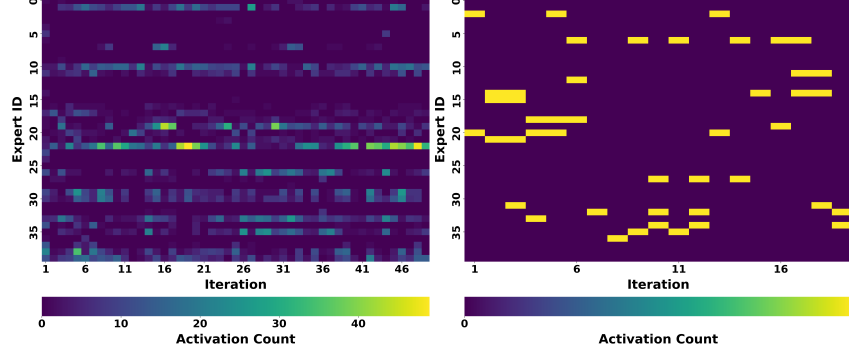


Figure 8: Activation frequency across iterations in SD is shown on the left, while the AR is shown on the right. It is much easier to estimate the light points where the experts are activated multiple times (hot experts).

Draft Model are α^l -Lipschitz and β^l -Lipschitz respectively [50]. Let W_r^l be the routing weight matrix at layer l with spectral norm C_R^l . The divergence in expert gating scores s^l (before Top- k selection) is bounded by:

$$\|s_t^l - s_{t+1}^l\| \leq C_R^l \cdot \delta_{in} \prod_{j=0}^{l-1} (1 + \sigma^j), \quad (23)$$

where $\sigma^j = \beta^j(1 + N\alpha^j)$ represents the layer-wise expansion factor:

Preliminaries. Let the hidden state update rule in the l -th Transformer layer be:

$$\mathbf{h}^{l+1} = \mathbf{h}^l + \text{FFN}^l(\mathbf{h}^l + \text{Attn}^l(\mathbf{h}^l)). \quad (24)$$

We assume the Lipschitz conditions for the sub-modules:

$$\|\text{Attn}^l(\mathbf{h}) - \text{Attn}^l(\mathbf{h}')\| \leq \alpha^l \|\mathbf{h} - \mathbf{h}'\|, \quad (25)$$

$$\|\text{FFN}^l(\mathbf{h}) - \text{FFN}^l(\mathbf{h}')\| \leq \beta^l \|\mathbf{h} - \mathbf{h}'\|. \quad (26)$$

Step 1: Layer-wise Divergence Propagation. Consider two input states \mathbf{h}_t^l and \mathbf{h}_{t+1}^l entering layer l . Let $\Delta^l = \|\mathbf{h}_t^l - \mathbf{h}_{t+1}^l\|$. Subtracting the update equations Eq. (24) for both states:

$$\|\mathbf{h}_t^{l+1} - \mathbf{h}_{t+1}^{l+1}\| \leq \|\mathbf{h}_t^l - \mathbf{h}_{t+1}^l\| + \beta^l (\|\mathbf{h}_t^l - \mathbf{h}_{t+1}^l\| + \|\text{Attn}^l(\mathbf{h}_t^l) - \text{Attn}^l(\mathbf{h}_{t+1}^l)\|) \quad (27)$$

$$\leq \Delta^l + \beta^l(\Delta^l + \alpha^l \Delta^l) \quad (28)$$

$$= (1 + \beta^l + \alpha^l \beta^l) \Delta^l. \quad (29)$$

Let $\sigma^l \triangleq \beta^l(1 + \alpha^l)$. The recurrence relation becomes:

$$\Delta^{l+1} \leq (1 + \sigma^l) \Delta^l. \quad (30)$$

Step 2: Unrolling the Recursion. Recursively applying the inequality from layer 0 (input embedding) to layer l :

$$\Delta^l \leq \Delta^0 \prod_{j=0}^{l-1} (1 + \sigma^j), \quad (31)$$

where $\Delta^0 = \delta_{in}$ is the initial divergence between the contexts.

Step 3: MoE Router Projection. In an MoE layer, the gating scores $s^l \in \mathbb{R}^E$ (before softmax and Top-K) are computed via a linear projection W_r^l :

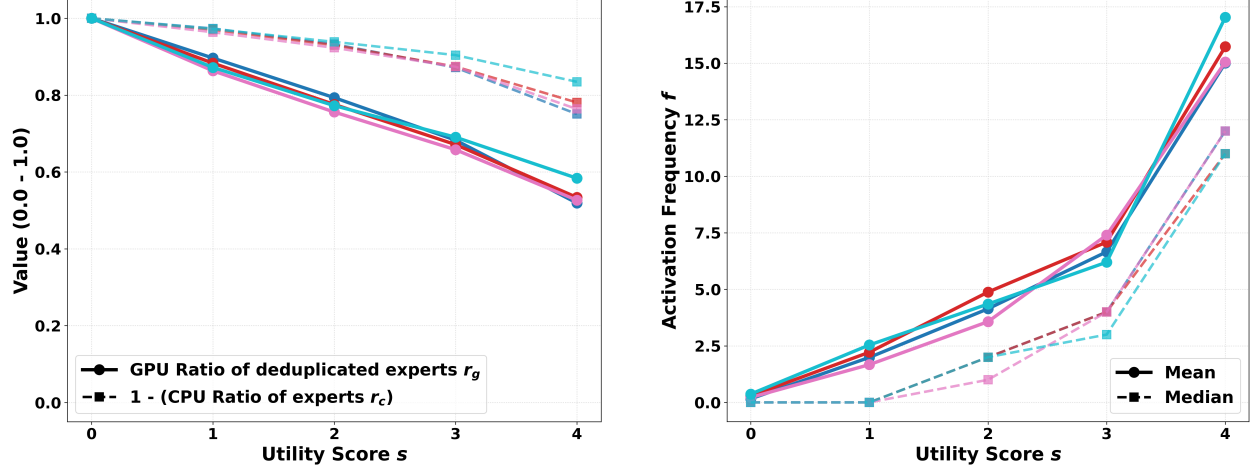
$$s^l = W_r^l \mathbf{h}^l. \quad (32)$$

The magnitude of the difference in gating scores is bounded by the spectral norm of the weight matrix $C_R^l = \|W_r^l\|_2$:

$$\|s_t^l - s_{t+1}^l\| = \|W_r^l(\mathbf{h}_t^l - \mathbf{h}_{t+1}^l)\| \quad (33)$$

$$\leq \|W_r^l\| \cdot \|\mathbf{h}_t^l - \mathbf{h}_{t+1}^l\| \quad (34)$$

$$= C_R^l \Delta^l. \quad (35)$$



(a) Utility score to the ratio of γk activated experts that can be processed on GPU, $1 - r_c$ (Dotted line) and the ratio of deduplicated activated experts to be processed on GPU in parallel, r_g (Solid line) for a single layer.

(b) Utility Score to the average value (Solid line) and median (Dotted line) of activation frequency. Experiment conducted on MT-Bench with $K = 4$ on Qwen models.

Figure 9: Relationship between utility score and activated frequency, ratio of activated experts, etc..

Conclusion. Substituting the unrolled bound for Δ^l , we obtain the final inequality:

$$\|\mathbf{s}_t^l - \mathbf{s}_{t+1}^l\| \leq C_R^l \cdot \delta_{in} \prod_{j=0}^{l-1} (1 + \sigma^j). \quad (36)$$

This confirms that the expert routing scores exist within a bounded region around the previous step’s scores, scaled by the depth of the network and the Lipschitz constraints of the layers. \square

Eq. 23 implies that activation frequency $f_{i,t}$ undergoes smooth transitions rather than abrupt jumps, validating the use of inertial transitions. Furthermore, since the bound depends on the layer-specific spectral norm C_R^l , the activation volatility varies across experts, necessitating the proposed Adaptive Boundary Calibration.

Eq. 23 demonstrates that the routing signal is Lipschitz continuous with respect to the input context. Since the gating scores \mathbf{h} determine the Top- k selection, a bounded $\|\Delta \mathbf{h}\|$ implies that the resulting activation frequency $f_{i,t}$ undergoes smooth transitions rather than abrupt jumps. This smoothness condition justifies our use of inertial discrete scoring (Score $s \rightarrow s \pm 1$) as a high-confidence estimator of future utility.

C Optimization Formulation & Solution for Heterogeneous Workload Balancer

C.1 Formulation Explanation

To illustrate Equation 7 and Equation 8, we first look at the two functions related to τ . As depicted in Figure. 9a, the ratio of γk activated experts processed on CPU $r_c(\tau)$ and the ratio of de-duplicated activated expert processed on GPU $r_g(\tau)$ remain stable in value for a given threshold k within a single layer. Therefore, this value can be learned from a warm up test.

To illustrate their relations with T_{CPU} and T_{GPU} , say an inference step that activates two experts per token with two draft tokens ($\gamma = 2$). If a layer forward pass prefetches expert No. 3 based on threshold τ , while the draft tokens activate experts {No. 0, No. 3} and {No. 2, No. 3}. Then $r_c(k) \approx 1 - \frac{2}{4}$ and $r_g(\tau) \approx 1/3$. The host calculation time would be the sum of computations for missed experts 0 and 2, taking time $r_c(\tau) \times 4 \times T_{cpu}^u$. The device processes the stacked hidden states of the identified experts concurrently, which only takes $r_g(\tau) \times 3 \times T_{gpu}^u$.

Besides, Eq. 10 imposes a strict constraint to prevent I/O bottlenecks. Specifically, the prefetching budget for each layer is bounded by the aggregate duration of computation and the corresponding drafting phase. By prioritizing the placement of hot experts on the limited device memory, the optimization forces the thresholding policy to align with the inter-device transmission bandwidth. Equation 12 enforces a strictly positive threshold ($\tau > 0$) to differentiate

our predictive approach from non-selective prefetching strategies. Regarding Eq. 11, minimizing the overhead is critical; querying the remaining memory $VRAM_{left}$ via `cudaMemGetInfo` entails non-negligible latency in CPU. Consequently, we can formulate an online linear programming problem to prioritize matching other constraints first, incorporating the memory constraint with latency-aware adjustments [51, 52].

Furthermore, Figure 9b empirically demonstrates that a higher score in utility estimator correlates with a higher frequency score in computation, thereby better utilizing the high-dimensional computational capacity of the GPU [53].

C.2 Solution Derivation

Since the domain of τ is restricted to integers $\tau \in [1, K]$, we determine the optimal τ^* by exploiting the structural properties of the objective function. First, we define the feasible set \mathcal{S} constrained by physical resources. Let the available computation window be $C_{window} = T_{total} + \gamma \cdot T_{draft}^u / L_{target}$. Based on the I/O (Eq. 10) and Memory (Eq. 11) constraints, the feasible set is determined by the range of prefetching volume $n(\tau)$:

$$\mathcal{S} = \{\tau \in \mathbb{Z} \mid \tau_{min} \leq \tau \leq \tau_{max}\} \subseteq [1, K] \quad (37)$$

where the bounds τ_{min} and τ_{max} are derived from the limits on $n(\tau)$ imposed by C_{window} and $VRAM_{left}$. The objective function is defined as the absolute difference between the device execution times:

$$f(\tau) = \left| \underbrace{r_c(\tau) \cdot \gamma \cdot k \cdot T_{cpu}^u}_{T_{cpu}(\tau)} - \underbrace{r_g(\tau) \cdot b \cdot T_{gpu}^u}_{T_{gpu}(\tau)} \right| \quad (38)$$

Since a higher threshold τ reduces the number of hot experts, the GPU allocation ratio $r_g(\tau)$ is monotonically decreasing, causing $T_{gpu}(\tau)$ to decrease. Conversely, the CPU allocation ratio $r_c(\tau)$ is monotonically increasing, causing $T_{cpu}(\tau)$ to increase. Consequently, the difference $T_{cpu}(\tau) - T_{gpu}(\tau)$ is strictly monotonic, rendering its absolute value $f(\tau)$ a **convex function** with respect to τ . Due to this **convexity**, the global minimum over the discrete set \mathcal{S} can be identified in $O(1)$ time. The optimal solution τ^* corresponds to either the integer closest to the theoretical intersection point τ_{cross} where $T_{cpu}(\tau_{cross}) = T_{gpu}(\tau_{cross})$, or one of the boundary points of \mathcal{S} if the intersection lies outside the feasible range:

$$\tau^* = \arg \min_{\tau \in \{\tau_{min}, \tau_{max}, \lfloor \tau_{cross} \rfloor, \lceil \tau_{cross} \rceil\} \cap \mathcal{S}} f(\tau) \quad (39)$$

If $\mathcal{S} = \emptyset$, we default to $\tau = K$ as a fallback strategy. Otherwise, this analytical approach ensures the exact optimal integer solution is obtained with minimal computational cost.

D Implementation Details of Unified Asynchronous Execution Engine

When it comes to the management of VRAM cache and score-based prefetching method, Figure 10 shows the details. Each expert ID is pushed into the queue labeled with corresponding score. With the online decision of threshold, the queue with lower label is filtered out. Then the experts are prefetched according to the ID reported in the queue from high to low. When prefetching is finished, each expert weight is tagged with a score and recorded in a set. When the expert is in used, the score is modified to $K + 1$, which we call a frozen expert, because under no circumstance should it be evicted. Due to the limited resources, most experts should be evicted right after calculation, and leave the space for layers to come. Therefore, we change these scores to 0, thus quickly recycled and refilled by other weights. All the experts weight is cache is recorded dynamically with a `set`, reaching an ideal efficiency with fine-grained lock usage.

We implement the management and scheduling system asynchronously atop `llama.cpp`, which native support CPU specific or GPU specific expert calculation. As shown in Figure 11, we hack a `ids_tensor` modification in backend, rewrite the expert calculation kernel: skip the calculation of expert with special label in `ids_tensor`. This modification is applied to each process in expert calculation in one layer forward, including $W_{up} \cdot x$, $W_{gate} \cdot x$, and $W_{down} \cdot x$. With a CUDA kernel joining up the result from the heterogeneous devices, we implement this process neatly without breaking the computation graph.

E Baseline Information

We compare MoE-SpAc against representative inference systems covering dense and MoE models, as well as different offloading and prediction strategies as follows:

- `Transformers Accelerate` [28] supports layer-wise parameter offloading via device maps.

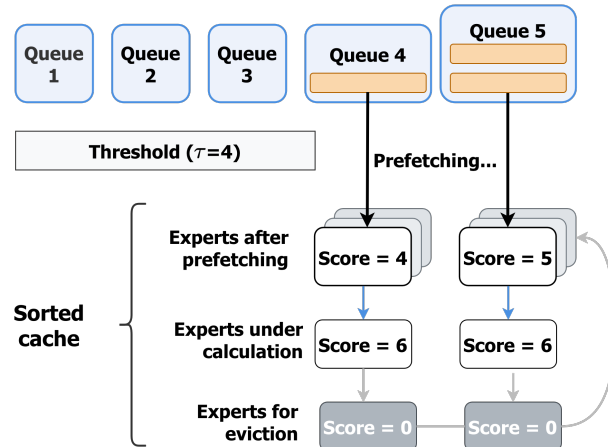


Figure 10: Scheduling and cache management of the MoE-SpAc in implementation when $K = 5$.

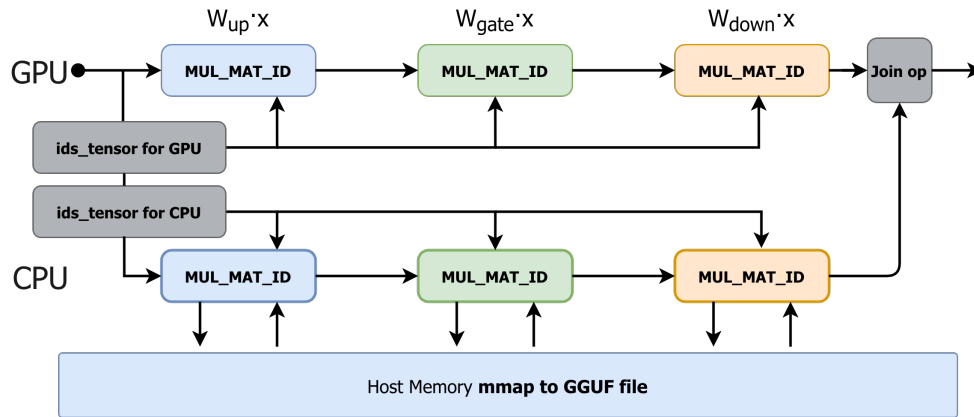


Figure 11: MoE-SpAc implementation atop llama.cpp, unchanged operators is omitted.

- vLLM [29] is a high-throughput inference engine that supports CPU offloading using a Least Recently Used (LRU) eviction policy.
- llama.cpp [30] is a lightweight inference engine optimized for constrained GPU environments.
- llama.cpp-w/ SD extends llama.cpp with speculative decoding.
- Mixtral Offloading [31] offloads expert weights between CPU and GPU while maintaining an LRU cache.
- MoE-Infinity [11] is a cost-effective MoE inference library that predicts expert activation paths and evicts experts based on least visit count.
- SP-MoE [32] predicts expert activation by directly using a draft model.
- Fate [33] predicts activated experts using the gating output of the subsequent layer and proactively offloads expert weights to target devices.
- HybriMoE [15] is a hybrid CPU-GPU inference framework that improves resource utilization through a heterogeneous scheduling and cache management system, implemented atop kTransformers.

F Illustration of Inference Pipelines

In Figure 12, we compare the pipeline of our proposed MoE-SpAc with other scheduling baselines. We can observe that speculative decoding with heterogeneous computation allows parallel scheduling. With load balancing from Section 3.3, we can achieve much less time elapsed compared with other expert-scheduling baselines.

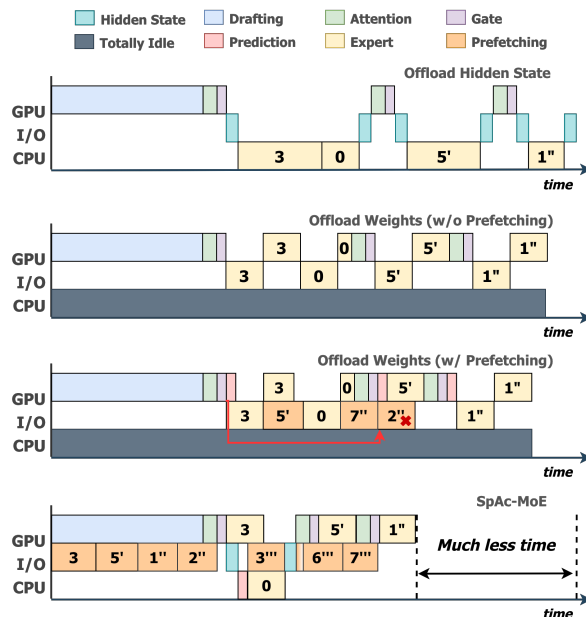


Figure 12: Comparison of MoE inference pipelines under Speculative Decoding (SD). 'GPU' and 'CPU' denote the compute device for expert layers, while prime notation (e.g., 1', 1'') indicates the layer depth. MoE-SpAc (bottom) minimizes pipeline bubbles via optimized heterogeneous scheduling.

G Related Works

Efficient MoE on Edge. MoE has emerged as a crucial architecture for scaling LLMs, prompting extensive research into optimizing its inference efficiency. Model compression techniques—including pruning [37, 38], quantization [39, 40], distillation [54, 55], and decomposition [56, 57]—have been successfully applied to MoEs. However, similar to their application in dense models, these methods inevitably trade generation quality for acceleration. In scenarios where MoEs exceed GPU memory capacity, system-level offloading becomes essential. While latency in large-batch regimes can be amortized via micro-batch pipelining [58, 59, 60, 61], low-latency inference for single-batch requests remains challenging. To address this, *on-demand loading* methods, such as Lina Li et al. [10] and ExpertFlow He et al. [42], exclusively utilize GPUs for expert computation. If an expert is not prefetched to the GPU, it must be loaded on demand. The downside of these approaches is the high I/O overhead, which causes prolonged GPU idling. *Expert Prefetching* [11, 41, 33] leverages historical activation patterns to preload experts, overlapping I/O with computation. Complementarily, *Expert Caching* [42, 43, 41] exploits the temporal locality of expert activation to retain experts in high-bandwidth memory, mitigating offloading overheads.

Speculative Decoding (SD). SD allows for lossless latency reduction by verifying multiple drafted tokens in parallel [17, 18, 62]. Recently, Zhang [63] provided a precise information-theoretic rationale for SD by quantifying the information surplus in hidden states. However, the efficiency of SD is highly sensitive to the operational intensity. As batch size increases, the system transitions from memory-bound to compute-bound, making the verification of speculated tokens prohibitively expensive [64, 65, 66, 67]. Conversely, for personal or edge usage where batch sizes are small, inference is strictly memory-bound. In this regime, the additional arithmetic operations required for SD verification are strictly encompassed by the memory retrieval time, making SD an ideal candidate for acceleration[44].

Heterogeneous Computing. Previous offloading techniques have primarily focused on reducing memory transfer overhead by offloading certain computations to the CPU[68]. For instance, PowerInfer[69] reduces GPU memory demand by executing less frequently activated neurons on the CPU, taking advantage of skewed activation patterns. Caraserve[70] addresses cold-start delays in LoRA serving by utilizing CPU assistance and employing rank-aware scheduling to reduce latency. However, they do not ensure skewed activations of neurons or parameter reuse. In the context of MoE models, techniques like Fiddler [12] and kTransformers [13] extend this concept by offloading expert layer computation to the CPU during cache misses. Specifically, when an expert is not in the GPU cache, the CPU executes the corresponding expert layer instead of loading it from memory. These approaches aim to optimize memory usage by exploiting CPU-GPU parallelism and mitigating the overhead of loading large models onto the GPU, but still remains a huge waste. HybriMoE[15] introduces a queue that re-orders experts by token count, dispatching hot

experts to the GPU and cold ones to the CPU. It uses a greedy algorithm to minimize per-layer computation cost and prefetches experts for the next layer during non-expert computations to further reduce on-demand loading pressure. But its greedy algorithm and scoring-based cache strategy lacks theoretical foundation, and miss some opportunities to further accelerate the inference.

Concurrent Works. Recent studies have begun to explore the intersection of Speculative Decoding and MoE. Huang et al. [45] analyzed the efficacy of SD for sparse MoE, yet their theoretical analysis relies on the assumption of uniformly activated experts, ignoring certain correlations among drafted tokens. System-oriented works like those by Wang et al. [46] and Zhuge et al. [59] utilize CPU resources primarily to interleave the execution of draft and target models to maximize throughput, rather than offloading specific experts to reduce latency. While Chen et al. [32] and Wang et al. [47] leverage information from the draft model for activation prediction, they overlook the continuous activation trends across iterations and remain constrained to GPU-centric execution, failing to fully unlock the potential of heterogeneous computing.

H Future Work and Limitations

Future Work. It is important to note that our work is orthogonal to a broad class of efforts aimed at accelerating speculative decoding itself. Techniques such as KV-cache compression and reuse [67], as well as retraining- or alignment-based methods that improve draft–target agreement [48], can be readily integrated with MoE-SpAc to further reduce both memory footprint and verification overhead, thereby improving end-to-end efficiency. In addition, self-speculation approaches [71], which eliminate the need for a separate draft model, can significantly reduce memory consumption and free additional GPU capacity for expert caching, effectively increasing the achievable expert cache ratio within our framework. Our workload balancer can further take KV cache offloading and scheduling into account [72, 73], to avoid overhead caused by KV cache from both draft model and target model.

Beyond standard MoE architectures, emerging sparse model designs open new opportunities for utility-guided scheduling. Advanced architectures such as Mixture-of-Lookup-Experts (MoLE) [74] and conditional memory systems like Engram [75] introduce new axes of sparsity and structured lookup mechanisms. These designs naturally expose richer and more stable access patterns, which could enable more accurate expert utility estimation and prefetching decisions. As models become increasingly sparse across parameters, activations, and memory accesses, the speculative-utility-based scheduling paradigm proposed in this work is expected to play an increasingly central role in efficient inference systems.

Limitations. Despite its effectiveness, our approach has several limitations. First, MoE-SpAc fundamentally relies on speculative decoding to provide informative, frequency-valued activation signals; when speculative decoding is ineffective (e.g., due to low acceptance rates or strict latency constraints), the benefits of speculative utility estimation are reduced. Second, the proposed system introduces additional scheduling and bookkeeping complexity, including utility tracking, online threshold optimization, and asynchronous execution management, which may incur nontrivial engineering overhead in practice. Finally, our evaluation focuses on single-GPU, batch-size-one edge scenarios; extending the framework to multi-GPU environments, higher batch sizes, or alternative interconnects remains an open direction for future work.